THE JOURNAL OF PHYSICAL CHEMISTRY C
A JOURNAL OF THE AMERICAN CHEMICAL SOCIETY

pubs.acs.org/JPCC

Article

Low-Threshold Amplified Spontaneous Emission from Defect-Passivated Quasi-2D Perovskites

Published as part of The Journal of Physical Chemistry C virtual special issue "The Physical Chemistry of Perovskites."

Deyue Zou, Xiaoyang Guo,* Zhiqiang Bao, Ying Lv, Tienan Wang, Baohua Zhang,* and Xingyuan Liu*

Cite This: *J. Phys. Chem. C* 2023, 127, 21841−21848

Read Online

ACCESS | Metrics & More | Article Recommendations | Supporting Information

ABSTRACT: Quasi-two-dimensional (quasi-2D) perovskites demonstrate outstanding optoelectronic performance among various perovskite materials. However, to fully leverage their potential for electrically pumped lasing, careful optimization remains imperative. Exploring the domain of quasi-2D perovskite amplified spontaneous emission (ASE) holds profound significance in achieving cost-effective, solution-processable green lasers. Challenges arise from the intrinsic uneven surfaces and numerous pinholes present in pristine quasi-2D perovskite films, leading to elevated levels of optical scattering and nonradiative recombination. In this study, perovskite films with significantly improved surface morphology, optical gain properties, and ASE performance were obtained through the introduction of Tween 80 (T80) for morphology control and defect passivation. Consequently, the nonradiative recombination rate of T80-treated perovskite films experiences a 10-fold reduction. Moreover, a strikingly low ASE threshold of 3.4 μJ cm^{-2}, accompanied by a 2-fold increase in the optical gain coefficient, has been achieved. This study demonstrates that the T80-treated quasi-2D perovskites have great promise in high-performance laser devices.

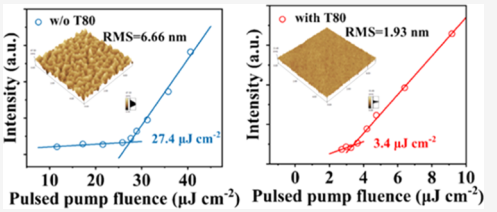

INTRODUCTION

Lasers hold significant roles across diverse fields, including industry, medicine, scientific research, and the military. Semiconductor lasers, owing to their small size, low power consumption, extended lifespan, efficiency, and ease of integration, offer great promise for applications in information storage, biological imaging, and sensors.[1−5] Inorganic semiconductors are used as the gain medium of conventional semiconductor lasers, but their preparation processes are complex and costly. As an emerging new gain media, perovskites have high absorption coefficient, superior carrier mobility, long carrier diffusion length, efficient fluorescence, and tunable wavelength.[6−11] Introducing quasi-two-dimensional (quasi-2D) perovskites—a subset of perovskites that integrate sizable hydrophobic organic cations into the framework of conventional three-dimensional (3D) perovskites (e.g., phenylethylammonium (PEA), butylamine (BA))—enhances their environmental stability.[12−16] The incorporation of organic cations contributes to heightened dielectric shielding and quantum effects within perovskite materials, thereby expediting the radiative recombination of excitons.[17−24] Notably, the spontaneous emergence of quantum well structures accelerates the energy transfer and facilitates the amplified spontaneous emission (ASE) of quasi-2D perovskites.[25]

ASE conventionally relies on a waveguide structure, a configuration sensitive to the roughness and thickness of the film.[26] A rougher surface topography can accentuate optical scattering, while a thinner film thickness might hinder the formation of an effective waveguide structure. Inorganic perovskites are prone to pinholes, poor morphology, and limited thickness in films due to the low solubility of CsX (X = Cl, Br, I).[27] Although vacuum thermal evaporation offers a means to control film thickness and enhance surface morphology, this method is more intricate and costly compared to solution-based approaches.[27−30] Consequently, the utilization of organic−inorganic hybrid quasi-2D perovskites holds notable advantages for generating thick and uniformly flat films. Various strategies such as the manipulation of organic cations,[31−34] the incorporation of additives,[35−37] recrystallization,[31,38,39] and surface modification[40] have been implemented to optimize film quality. However, recrystallization often entails the use of substantial organic solvents to establish a conducive atmosphere, with processing times spanning from 1 h to 2 weeks, rendering the approach relatively cumbersome and environmentally unfriendly.[31] In contrast, the introduction of additives into perovskite

Received: August 30, 2023
Revised: October 13, 2023
Accepted: October 13, 2023
Published: October 27, 2023

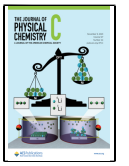

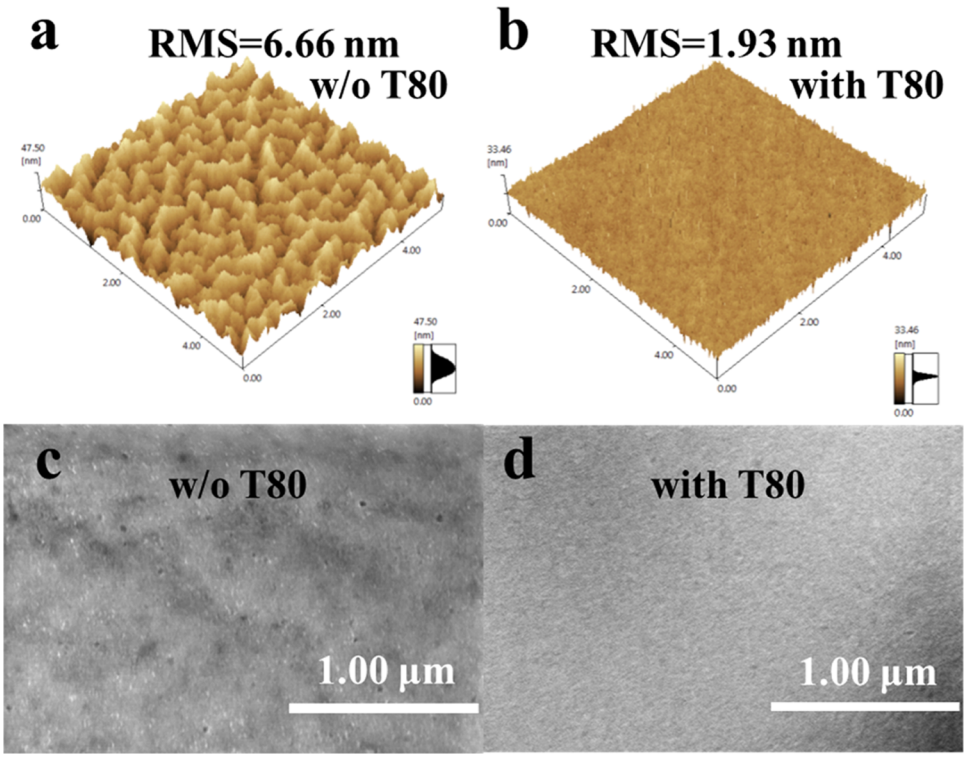

Figure 1. AFM images of perovskite films (a) without and (b) with T80. SEM images of perovskite films (c) w/o and (d) with T80.

precursor solutions has emerged as a simpler and much quicker way for enhancing the quality of thin films. This approach not only passivates defects but also augments the luminous performance of the films, as demonstrated in the context of perovskite light-emitting diodes. Nonetheless, while additives exhibit the potential to improve defect passivation and enhance luminescence, their impact on the optical gain performance of perovskite thin films remains an area that requires further exploration.

In this study, we demonstrate the enhanced luminescence characteristics of perovskite films through the incorporation of Tween 80 (T80). The introduction of T80 as an additive improved the film's morphology, leading to reduced light losses. The perovskite film treated with T80 exhibits heightened fluorescence intensity while maintaining the same phase distribution. This improvement in luminescence is achieved without alteration of the phase composition. By effectively passivating defects, the perovskite film treated with T80 experiences a notable 55% reduction in defect density. This defect reduction contributes to the suppression of nonradiative recombination within the perovskite films, thereby facilitating improvements in the amplified spontaneous emission. The gain coefficient of the film, treated with T80, increases from 62 to 120 cm^{-1}, signifying a substantial enhancement. All of these improvements lead to the attainment of a significantly reduced ASE threshold of 3.4 μJ cm^{-2}, which is nearly 1 order of magnitude lower than the initial threshold of 27.4 μJ cm^{-2}. This work presents an effective and practical approach to enhancing the ASE performance of quasi-2D perovskites, and will provide feasible insights for the design of perovskite-based laser devices.

MATERIALS AND METHODS

Materials. Lead bromide (PbBr), phenylethylammonium bromide (PEABr), formamidinium bromide (FABr), and PEDOT:PSS were purchased from Xi'an Polymer Light Technology Corp. Tween 80 was purchased from Sigma-Aldrich. All materials were used directly without further purification.

Perovskite Film Fabrication and Characterization. The powders of PEABr, FABr, and $PbBr_2$ (molar ratio of 1:3:3) were added into an anhydrous DMF solvent containing T80 and stirred at 50 °C for 4 h. A transparent perovskite precursor solution with a concentration of 0.4 M was obtained. The concentrations of T80 in DMF were 1, 3, 5, and 7 mg mL^{-1}, respectively. The mixtures were then spin-coated on the glass at 4500 r.p.m. for 30 s. During the spin-coating process, 0.20 mL of absolute ethyl acetate was dropped onto the perovskite precursor layer at the fifth second. The substrates were baked on a hot plate at 120 °C for 10 min. The morphology of the perovskite films was characterized by scanning electron microscopy (SEM) (Hitachi 4800). The surface roughness was analyzed by atomic force microscopy (AFM) on a Shimadzu SPA-9700. The absorption spectra of perovskite films were measured on a Shimadzu UV-3101PC. The photoluminescence (PL) spectra of perovskite films were measured by using a Hitachi F-7000 fluorescence spectrometer. Time-resolved PL spectra of perovskite films were measured on an Edinburgh FLS920 spectrometer. The X-ray diffraction (XRD) patterns of perovskite films were measured using a Rigaku SmartLab. Pulse optical pumping ASE measurement was performed by using a CryLas GmbH Nd:YAG laser at 355 nm with a pulse width of 1 ns and a repetition rate of 50 Hz. In order to fit the defect density, the films were optically pumped by using a CryLas GmbH Nd:YAG laser at 355 nm, and the PL spectra were collected

https://doi.org/10.1021/acs.jpcc.3c05840
J. Phys. Chem. C 2023, 127, 21841−21848

from the side. The stripe pumping beam was focused by a cylindrical lens, and the pump fluence was tuned by calibrated neutral density filters. Temperature-dependent PL spectra were collected using a Horiba iHR550 system equipped with 405 nm solid-state lasers and a helium-flow cryostat.

RESULTS AND DISCUSSION

In this study, we employed T80 as a passivator to create perovskite films. By using additives with hydroxyl functional groups, we can effectively enhance the passivation of defect sites, particularly the Pb^{2+} vacancies.[41,42] The molecular structure of T80, illustrated in Figure S1, highlights its numerous hydroxyl groups. These hydroxyl groups, due to their Lewis basicity, establish interactions with Pb^{2+} ions. This interaction leads to the development of a smoother surface morphology with reduced defects in the film. As a result of our optimization efforts, the thin film achieved significant potential for application in perovskite lasers.

Figure 1a,b exhibits AFM images of perovskite films both without (w/o) T80 and with T80 (5 mg mL^{-1}). The root-mean-square (RMS) value of the perovskite film, upon the addition of T80, decreased from 6.66 to 1.93 nm. These figures illustrate that the inclusion of T80 influences the growth of the perovskite crystals, resulting in a smoother overall morphology. To investigate the impact of varying concentrations of T80 on perovskite films, we also prepared films with T80 concentrations of 1, 3, and 7 mg mL^{-1} (Figure S2). As depicted in the figures, the incorporation of T80 significantly reduced the surface roughness of the perovskite films. Notably, the perovskite film with T80 at 1 mg mL^{-1} displays an RMS value of 1.82 nm, while this value increases to 2.07 nm when T80 is added up to 7 mg mL^{-1}. This finding suggests that the concentration of added T80 impacts its efficacy in enhancing film morphology, and excessive T80 might not be advantageous for regulating film structure. The achievement of a flat surface reduces optical scattering, which is advantageous for achieving ASE. Figure S3 illustrates the PL of perovskite films with varying T80 concentrations. Evidently, the addition of T80 results in perovskite films with enhanced fluorescence. This enhancement can be attributed to T80's ability to passivate defects in the perovskite film, promoting radiative recombination. Considering both the refined surface morphology and intensified fluorescence, we selected a T80 concentration of 5 mg mL^{-1} for subsequent experiments. In Figure 1c,1d, SEM images of perovskite films without T80 and with T80 treatment are presented. These SEM images corroborate the morphology observed by AFM (Figure 1). The introduction of T80 not only contributes to a smoother film surface but also diminishes the occurrence of pinholes. This effect is likely due to T80's presence at grain boundaries, acting as a passivator and binding the perovskite grains together.[43] Figure S4 shows the SEM image of the perovskite film at a higher magnification, which demonstrates more intuitively that the addition of T80 optimizes the morphology of the film. The perovskite film containing T80 measures approximately 100 nm in thickness (Figure S5), which is nearly identical with the thickness of the original film. This demonstrates that the addition of T80 essentially does not alter the film's thickness.

Figure 2a shows the ultraviolet−visible (UV−Vis) absorption spectra and PL spectra of perovskite films with and w/o T80. The PL intensity of the perovskite film with T80 is significantly enhanced, reaching an enhancement of approximately 2.12 times compared to the pristine film. This boost in PL can be attributed to T80's ability to mitigate surface defects, thereby suppressing nonradiative recombination processes. The absorption spectrum of the perovskite film with T80 does not exhibit absorption peaks from other phases, indicating that T80 addition does not influence the quasi-2D perovskite phases. It is worth noting that both the absorption and the PL curves exhibit a blue shift. Figure S6 shows the normalized PL spectra of the perovskite film with T80 and w/o T80. The PL peak position of the perovskite film with T80 shifts from 531 to 527 nm. This blue shift in both PL and absorption spectra can be attributed to the smaller grain size in the perovskite film with T80, as supported by the XRD patterns of the perovskite films presented in Figure 2b. The two prominent XRD pattern peaks at 14.8 and 29.7° correspond to the [100] and [200] crystal planes, respectively. Additionally, two weak peaks at 21.6 and 33.3° correspond to [110] and [210] planes, respectively.[44−46] The growth of perovskite crystals is predominantly along the horizontal direction.[47,48] Comparing the peak positions of the XRD spectra between the perovskite films with and without T80, they remain nearly identical. This observation suggests that the crystal structure of the perovskite has not undergone any significant changes due to the addition of T80. Notably, the intensity of the XRD pattern does not exhibit an increase, indicating that the introduction of T80 does not lead to an enhancement of the perovskite's crystallinity. Analyzing the full width at half-maximum (FWHM) of the XRD peak at 14.8°, the perovskite film without T80 has a FWHM of 0.67°, while the film with T80 has a FWHM of 0.73°. According to the Scherrer formula, this increase in the FWHM for the T80-treated film implies a reduction in grain size. Consequently, the addition of T80 induces the growth of perovskite crystals into smaller grains. Figure 2c presents the PL quantum yield (PLQY) of perovskite films with and w/o T80. The PLQY of the perovskite film experiences a substantial increase of 4.7 times, rising from 9% (w/o T80) to 51% upon T80 incorporation. Figure 2d displays the fluorescence lifetimes (τ_{avg}) of the perovskite films. The fluorescence lifetime of the

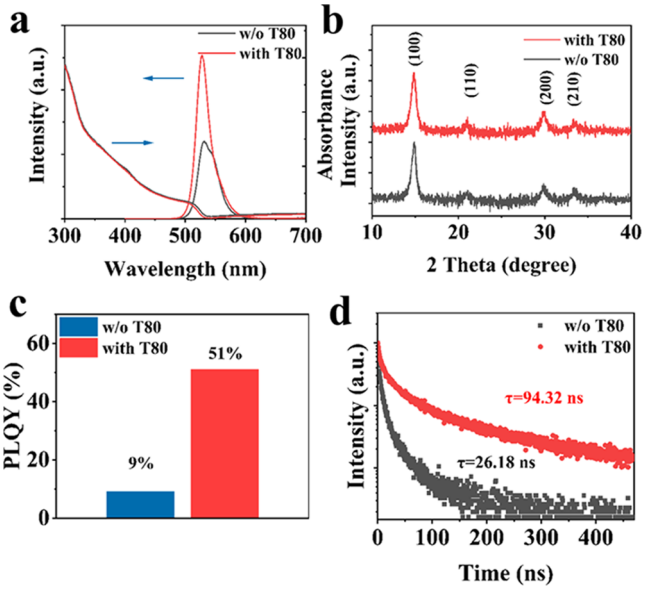

Figure 2. (a) Absorption and PL spectra, (b) XRD, (c) PLQY, and (d) fluorescence lifetime of perovskite films with and w/o T80.

https://doi.org/10.1021/acs.jpcc.3c05840
J. Phys. Chem. C 2023, 127, 21841−21848

perovskite film extends from 26.18 ns without T80 to 94.32 ns with T80 utilization. This extension in τ_{avg} indicates a reduction in the nonradiative recombination rates within the perovskite films. The relationship between τ_{avg} and PLQY can be expressed using an equation that describes the nonradiative recombination rate and radiative recombination rate

$$\tau_{avg} = \frac{1}{K_r + K_{nr}} \quad (1)$$

$$\mathrm{PLQY} = \frac{K_r}{K_r + K_{nr}} \quad (2)$$

$$K_{nr} = \frac{1 - \mathrm{PLQY}}{\tau_{avg}} \quad (3)$$

where K_r is the radiative recombination rate and K_{nr} is the nonradiative recombination rate. Obviously, the K_{nr} of a film exhibits an inverse relationship with its PLQY and τ_{avg}. Both an increased PLQY and an extended lifetime contribute to a decrease in the nonradiative recombination rate. For the perovskite film w/o T80, the nonradiative recombination rate is calculated as 3.47×10^{-7} s^{-1}. In contrast, for the perovskite film with T80, the nonradiative recombination rate is significantly lower at 5.0×10^{-8} s^{-1}, which is an order of magnitude decrease. This drastic reduction indicates that the addition of T80 effectively diminishes the extent of nonradiative recombination. According to the formula, the radiative recombination rate was also calculated. The radiative recombination rate for the perovskite film with T80 is 5.37×10^{-7} s^{-1}, while for the film w/o T80, it is 3.52×10^{-7} s^{-1}. The addition of T80 resulted in a 9.6 times increase in the ratio of radiative to nonradiative recombination rates. As a result of adding T80, the ratio of radiative to nonradiative recombination rates increases by a factor of 9.6. This underlines T80's effective role as a passivator in suppressing nonradiative recombination. Figures S7 and S8 show the PLQY and fluorescence lifetime of perovskite films doped with varying concentrations of T80. It is evident that the PLQY of the perovskite film increases from 9 to 83% as the T80 concentration increases. Additionally, the perovskite film's fluorescence lifetime extends to 96.9 ns with increased T80 concentration. Table S1 provides the fitting results for the nonradiative recombination rate. Within a certain range, the introduction of T80 effectively inhibits nonradiative recombination while simultaneously promoting accelerated radiative recombination, which proves beneficial for achieving ASE in perovskite lasers.

To gain a deeper understanding of the intrinsic characteristics of excitons in perovskite films, we performed temperature-dependent PL measurements using a continuous flow helium cryostat. Figure 3a,b presents the temperature-dependent PL spectra of perovskite films without T80 and with T80, respectively. As the temperature ascends from 80 to 300 K, the PL intensity progressively diminishes, signifying the occurrence of thermal quenching in the perovskite's PL emission. With the increase of temperature, the PL peaks of both perovskite films show a similar trend: they undergo a blue shift, FWHM broadens, and the PL intensity decreases. In essence, the shift in the PL peak can be attributed to the lattice's thermal expansion effect and the influence of exciton−phonon coupling. While exciton−phonon coupling tends to induce a red shift in the PL peak, the observed blue shift in the PL

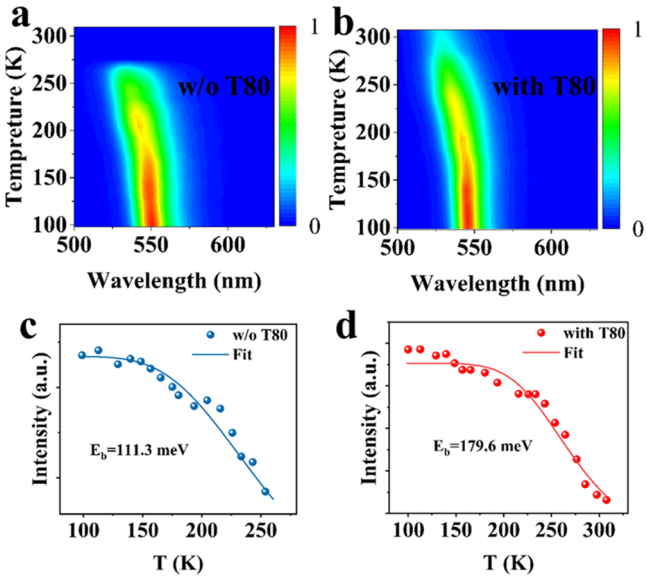

Figure 3. 2D pseudocolor plot of the temperature-dependent PL spectra of the perovskite films (a) without and (b) with T80. Temperature-dependent PL intensity of the perovskite films (c) w/o and (d) with T80.

spectrum is primarily a result of lattice thermal expansion.[49] For perovskites, the exciton binding energy (E_b) serves as an indicator of charge transfer and the probability of exciton dissociation. Figure 3c,3d illustrates the temperature-dependent behavior of PL intensity for perovskite films without T80 and with T80, respectively. To calculate the exciton binding energy (E_b), we can fit the PL intensity using the Arrhenius equation

$$I(T) = I_0 / \left(1 + A \exp\left(-\frac{E_b}{k_B T}\right)\right) \quad (4)$$

where I_0 and k_B are the PL intensity at 0 K and Boltzmann's constant, respectively. Based on the fitting results, the E_b of the pristine perovskite film is measured at 111.3 meV, while the perovskite film with T80 shows an E_b of 179.6 meV. The E_b of the perovskite film with T80 significantly surpasses the perturbation energy at room temperature (~26 meV), which facilitates the generation and recombination of excitons.

Furthermore, we compared the ASE of these two films under nanosecond pulsed laser pumping. The quasi-2D perovskite films were pumped using a 355 nm nanosecond pulsed laser with a stripe size of 300 μm × 6 mm. The ASE properties of the perovskite film without T80 are shown in Figure 4a,4c. Figure 4a shows the change of the PL spectrum of the perovskite film under a pump fluence of 25.8−40.6 μJ cm^{-2}. When the pump fluence is less than 27.4 μJ cm^{-2}, the PL spectrum with a central wavelength of 535 nm can be observed. With the increase of pump fluence, the intensity of PL spectrum is enhanced. When the pump fluence exceeds 27.4 μJ cm^{-2}, the PL intensity increases nonlinearly, and a narrow and high peak appears at 544 nm. The shift of PL peak reflects the transition from stimulated emission to ASE. Figure 4c provides a more intuitive representation of the relationship between the PL intensity and FWHM for perovskite films with or without T80 at different pump fluences. With the nonlinear enhancement of fluorescence intensity, the FWHM of PL decreased from 40 to 2.8 nm. By fitting the data points of PL

https://doi.org/10.1021/acs.jpcc.3c05840
J. Phys. Chem. C 2023, 127, 21841−21848

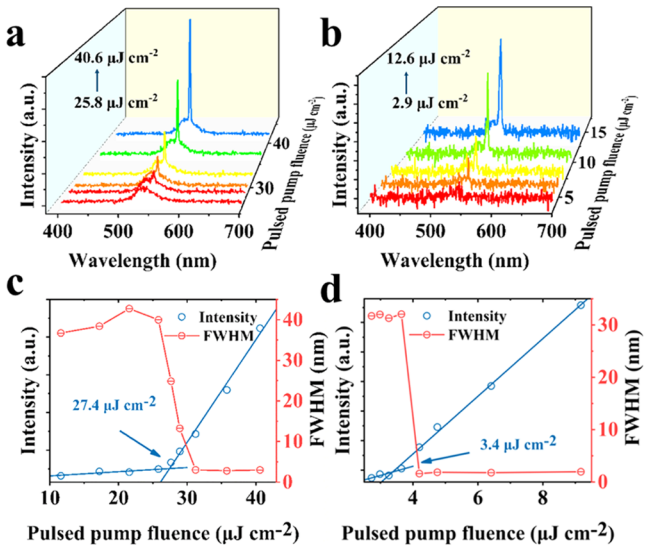

Figure 4. Emission spectra of perovskite films (a) with and without T80 and (b) with T80 at different pump fluence. The output intensity and FWHM of the perovskite films (c) w/o and (d) with T80 as a function of the pump fluence.

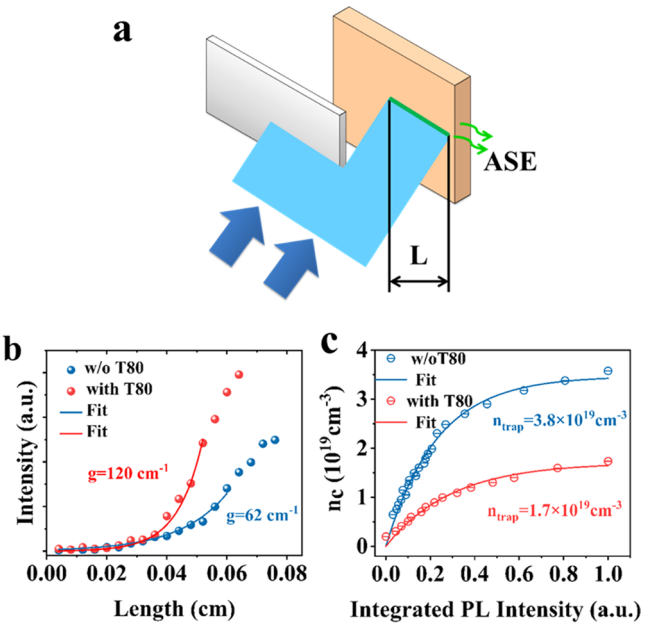

Figure 5. (a) Variable stripe length experiment for the estimation of modal net gain for the perovskite films. (b) PL intensity of the perovskite films with and w/o T80 as a function of stripe length under the energy densities of 1.5 P_{th} of the two films. (c) Integrated PL intensity as a function of photon-generated exciton density within the low excitation range.

intensities into two distinct ranges, we can derive two lines characterized by different slopes. The point at which these two fitted lines intersect corresponds to the pump threshold (P_{th}) for achieving ASE. The ASE properties of the perovskite film with T80 are shown in Figure 4b,d. As the pump fluence increases from 2.9 to 12.6 μJ cm^{-2}, the PL spectrum of the perovskite film with T80 appears as a narrowed peak at 547 nm, and its FWHM narrows from 32 to 1.7 nm. With the passivation effect of the additive T80, the perovskite film successfully attained an exceptionally low threshold of 3.4 μJ cm^{-2}. This achievement represents a substantial reduction of 7 times compared to the initial threshold of 27.4 μJ cm^{-2}. Notably, this film showcases enhanced photophysical characteristics, including a diminished P_{th} and a narrower FWHM for ASE.

When perovskite films are evaluated for use in ASE, the optical gain coefficient becomes a crucial parameter for assessing their optical waveguide performance. For a more comprehensive evaluation of the optical gain characteristics, the variable stripe length (VSL) method is employed to measure the net gain of the perovskite films. The experimental setup utilized for this test is depicted in Figure 5a,[50−52] where a laser is used to form a variable-length strip on the surface of the sample. As shown in Figure 5b, the PL intensity dependent on the fringe length can be obtained by adjusting the slit. The effective optical gain (g) can be determined using the following equation, which establishes a relationship between the output intensity (I) and the length of the excited strip (L)[53,54]

$$I = I_0(e^{gL} - 1)/g \tag{5}$$

wherein the term I_0 represents the rate of spontaneous emission per unit volume. At a pump fluence of 1.5 times the P_{th}, the gain coefficient of the untreated perovskite film is ∼62 cm^{-1}. In contrast, for the perovskite film passivated with T80, the gain coefficient notably increases to ∼120 cm^{-1}. This enhancement represents a substantial increase of 1.93 times compared with the original film's gain coefficient. The increased gain coefficient leads to a large decrease in the threshold for perovskite films. It is well known that nonradiative recombination channels such as defect states, Auger recombination, and phonon scattering hinder optical gain. In order to find out the reasons for the increase of gain coefficient and the mechanism of T80 suppression of nonradiative recombination of perovskite thin films, we analyzed the carrier dynamics of perovskite thin films. Defects are generally considered to be fast, nonradiative pathways that compete with radiative recombination.[55] The dynamics of the photogenerated carrier density (n_c) can be described by the following differential equation[38]

$$\frac{dn_c(t)}{d_t} = -\sum_i a_i n_c(t) n_{TP}^i(t) - \frac{n_c(t)}{\tau_0} \tag{6}$$

$$\frac{dn_{TP}^i(t)}{d_t} = -a_i n_c(t) n_{TP}^i(t) \tag{7}$$

where a_i is the coefficient, which represents the ability of the trap states to capture carriers. n_{TP}^i is the density of the trap states. Thus, the relationship between the integrated PL intensity (I_{PL}) and the initial photogenerated charge carrier density $n_c(0)$ can be expressed as[38]

$$n_c(0) = n_{TP}(0)(1 - e^{-a\tau_0 I_{PL}/k}) + \frac{I_{PL}}{k} \tag{8}$$

where τ_0 is the lifetime of carriers under low excitation density, k is a constant, $n_c(0)$ is the carrier density, which can be found in the Supporting Information. Figure 5c shows the relationship between $n_c(0)$ and I_{PL}, and the defect density can be fitted, as shown by eq 8. It can be calculated that the defect density of the perovskite film passivated by T80 is 1.7 × 10^{19} cm^{-3}. In contrast, the pristine perovskite film exhibits a defect density of 3.8 × 10^{19} cm^{-3}, which is 2.2 times higher than that of the perovskite film with T80. This contrast indicates that the addition of T80 greatly reduces the defect density,

https://doi.org/10.1021/acs.jpcc.3c05840
J. Phys. Chem. C 2023, 127, 21841−21848

consequently suppressing the nonradiative recombination processes. We also measured the dark current of hole-only devices with the structure of ITO/PEDOT:PSS/perovskite/MoO_3/Ag under different bias voltages and analyzed the defect density by using the following equation

$$N_{\text{defects}} = \frac{2\varepsilon_0\varepsilon_r V_{\text{TFL}}}{qL^2} \quad (9)$$

ε_0 and ε_r refer to vacuum dielectric constant and relative dielectric constant, respectively, q refers to electron charge, L refers to the thickness of the perovskite film, and V_{TFL} is transition voltage and is shown in Figure S9. V_{TFL} decreases from 0.33 to 0.15 V, which indicates the decrease in defect density of the perovskite film with T80 and demonstrates the positive role of T80 in defect passivation in perovskite films. This reduction in defect density plays a pivotal role in facilitating low-threshold ASE.

CONCLUSIONS

In summary, we introduced the use of additive T80 as an effective strategy for enhancing the ASE properties of quasi-2D perovskite films. The treatment with T80 yielded a smoother surface morphology for the perovskite film, marked by a reduction in the occurrence of pinholes. This smooth morphology results in decreased optical scattering and suppression of defect formation. Consequently, the defect density of the perovskite film is lowered from 3.8×10^{19} to 1.7×10^{19} cm^{-3}, and the nonradiative recombination rate is reduced by an order of magnitude. As a culmination of these effects, an ultralow ASE threshold of 3.4 μJ cm^{-2} is achieved, marking a remarkable 87.6% decrease compared to the original threshold of 27.4 μJ cm^{-2}. This achievement not only showcases the potential of T80 treatment for perovskite lasers but also offers valuable insights into the advancement and application of perovskite-based laser technologies.

ASSOCIATED CONTENT

Supporting Information

The Supporting Information is available free of charge at https://pubs.acs.org/doi/10.1021/acs.jpcc.3c05840.

Molecular structure of Tween 80; AFM images of perovskite films; PL spectra of perovskite films with different T80 concentrations; SEM characterizations; normalized PL spectra; PLQY and fluorescence lifetime of perovskite films with different T80 concentrations; current density−voltage curves for hole-only devices; summary table of nonradiative recombination rates; and calculation of carrier density (PDF)

AUTHOR INFORMATION

Corresponding Authors

Xiaoyang Guo − *State Key Laboratory of Luminescence and Applications, Changchun Institute of Optics, Fine Mechanics and Physics, Chinese Academy of Sciences, Changchun 130033, P. R. China;* orcid.org/0000-0003-0259-137X; Email: Email: guoxy@ciomp.ac.cn

Baohua Zhang − *Center for Advanced Analytical Science, c/o School of Chemistry and Chemical Engineering, Guangzhou Key Laboratory of Sensing Materials & Devices, Guangzhou University, Guangzhou 510006, China;* orcid.org/0000-0001-7017-2594; Email: Email: ccbhzhang@gzhu.edu.cn

Xingyuan Liu − *State Key Laboratory of Luminescence and Applications, Changchun Institute of Optics, Fine Mechanics and Physics, Chinese Academy of Sciences, Changchun 130033, P. R. China;* orcid.org/0000-0002-9681-1646; Email: Email: liuxy@ciomp.ac.cn

Authors

Deyue Zou − *State Key Laboratory of Luminescence and Applications, Changchun Institute of Optics, Fine Mechanics and Physics, Chinese Academy of Sciences, Changchun 130033, P. R. China; University of Chinese Academy of Sciences, Beijing 100049, P. R. China*

Zhiqiang Bao − *State Key Laboratory of Luminescence and Applications, Changchun Institute of Optics, Fine Mechanics and Physics, Chinese Academy of Sciences, Changchun 130033, P. R. China; University of Chinese Academy of Sciences, Beijing 100049, P. R. China*

Ying Lv − *State Key Laboratory of Luminescence and Applications, Changchun Institute of Optics, Fine Mechanics and Physics, Chinese Academy of Sciences, Changchun 130033, P. R. China;* orcid.org/0000-0003-1649-5258

Tienan Wang − *State Key Laboratory of Luminescence and Applications, Changchun Institute of Optics, Fine Mechanics and Physics, Chinese Academy of Sciences, Changchun 130033, P. R. China*

Complete contact information is available at: https://pubs.acs.org/10.1021/acs.jpcc.3c05840

Notes

The authors declare no competing financial interest.

ACKNOWLEDGMENTS

This work was supported by the National Science Foundation of China Nos. 62035013, 62175235, 51973208, 61975256, 52211530094, the Jilin Province Science and Technology Research Project (20220201091GX, 20220201064GX), Natural Science Foundation of Guangdong Province (2021A1515010510), and Guangzhou Science and Technology Plan Project (202102010409).

REFERENCES

(1) Lei, L.; Dong, Q.; Gundogdu, K.; So, F. Metal Halide Perovskites for Laser Applications. *Adv. Funct. Mater.* **2021**, *31*, No. 2010144.

(2) Liu, Z.; Huang, S.; Du, J.; Wang, C.; Leng, Y. Advances in Inorganic and Hybrid Perovskites for Miniaturized Lasers. *Nanophotonics* **2020**, *9*, 2251−2272.

(3) Wei, Q.; Li, X.; Liang, C.; Zhang, Z.; Guo, J.; Hong, G.; Xing, G.; Huang, W. Recent Progress in Metal Halide Perovskite Micro- and Nanolasers. *Adv. Opt. Mater.* **2019**, *7*, No. 1900080.

(4) Wang, K.; Wang, S.; Xiao, S.; Song, Q. Recent Advances in Perovskite Micro- and Nanolasers. *Adv. Opt. Mater.* **2018**, *6*, No. 1800278.

(5) Zhang, Q.; Su, R.; Du, W.; Liu, X.; Zhao, L.; Ha, S. T.; Xiong, Q. Advances in Small Perovskite-Based Lasers. *Small Methods* **2017**, *1*, No. 1700163.

(6) Jiang, Y.; Cui, M.; Li, S.; Sun, C.; Huang, Y.; Wei, J.; Zhang, L.; Lv, M.; Qin, C.; Liu, Y.; Yuan, M. Reducing the Impact of Auger Recombination in Quasi-2d Perovskite Light-Emitting Diodes. *Nat. Commun.* **2021**, *12*, No. 336.

(7) Zhao, B.; Bai, S.; Kim, V.; Lamboll, R.; Shivanna, R.; Auras, F.; Richter, J. M.; Yang, L.; Dai, L.; Alsari, M.; et al. High-Efficiency Perovskite−Polymer Bulk Heterostructure Light-Emitting Diodes. *Nat. Photonics* **2018**, *12*, 783−789.

(8) Byun, J.; Cho, H.; Wolf, C.; Jang, M.; Sadhanala, A.; Friend, R. H.; Yang, H.; Lee, T. W. Efficient Visible Quasi-2d Perovskite Light-Emitting Diodes. *Adv. Mater.* **2016**, *28*, 7515−7520.
(9) He, C.; Liu, X. The Rise of Halide Perovskite Semiconductors. *Light: Sci. Appl.* **2023**, *12*, No. 15.
(10) Zhang, D.; Fu, Y.; Zhan, H.; Zhao, C.; Gao, X.; Qin, C.; Wang, L. Suppressing Thermal Quenching Via Defect Passivation for Efficient Quasi-2d Perovskite Light-Emitting Diodes. *Light: Sci. Appl.* **2022**, *11*, No. 69.
(11) Zhang, L.; Sun, C.; He, T.; Jiang, Y.; Wei, J.; Huang, Y.; Yuan, M. High-Performance Quasi-2d Perovskite Light-Emitting Diodes: From Materials to Devices. *Light: Sci. Appl.* **2021**, *10*, No. 61.
(12) Xu, W.; Hu, Q.; Bai, S.; Bao, C.; Miao, Y.; Yuan, Z.; Borzda, T.; Barker, A. J.; Tyukalova, E.; Hu, Z.; et al. Rational Molecular Passivation for High-Performance Perovskite Light-Emitting Diodes. *Nat. Photonics* **2019**, *13*, 418−424.
(13) Miao, Y.; Ke, Y.; Wang, N.; Zou, W.; Xu, M.; Cao, Y.; Sun, Y.; Yang, R.; Wang, Y.; Tong, Y.; et al. Stable and Bright Formamidinium-Based Perovskite Light-Emitting Diodes with High Energy Conversion Efficiency. *Nat. Commun.* **2019**, *10*, No. 3624.
(14) Li, C.; Wang, N.; Guerrero, A.; Zhong, Y.; Long, H.; Miao, Y.; Bisquert, J.; Wang, J.; Huettner, S. Understanding the Improvement in the Stability of a Self-Assembled Multiple-Quantum Well Perovskite Light-Emitting Diode. *J. Phys. Chem. Lett.* **2019**, *10*, 6857−6864.
(15) Yang, M.; Wang, N.; Zhang, S.; Zou, W.; He, Y.; Wei, Y.; Xu, M.; Wang, J.; Huang, W. Reduced Efficiency Roll-Off and Enhanced Stability in Perovskite Light-Emitting Diodes with Multiple Quantum Wells. *J. Phys. Chem. Lett.* **2018**, *9*, 2038−2042.
(16) Chen, Y.; Sun, Y.; Peng, J.; Tang, J.; Zheng, K.; Liang, Z. 2d Ruddlesden-Popper Perovskites for Optoelectronics. *Adv. Mater.* **2018**, *30*, No. 1703487.
(17) Yuan, S.; Wang, Z. K.; Xiao, L. X.; Zhang, C. F.; Yang, S. Y.; Chen, B. B.; Ge, H. T.; Tian, Q. S.; Jin, Y.; Liao, L. S. Optimization of Low-Dimensional Components of Quasi-2d Perovskite Films for Deep-Blue Light-Emitting Diodes. *Adv. Mater.* **2019**, *31*, No. 1904319.
(18) Liu, Y.; Cui, J.; Du, K.; Tian, H.; He, Z.; Zhou, Q.; Yang, Z.; Deng, Y.; Chen, D.; Zuo, X.; et al. Efficient Blue Light-Emitting Diodes Based on Quantum-Confined Bromide Perovskite Nanostructures. *Nat. Photonics* **2019**, *13*, 760−764.
(19) Lee, H. D.; Kim, H.; Cho, H.; Cha, W.; Hong, Y.; Kim, Y. H.; Sadhanala, A.; Venugopalan, V.; Kim, J. S.; Choi, J. W.; et al. Efficient Ruddlesden−Popper Perovskite Light-Emitting Diodes with Randomly Oriented Nanocrystals. *Adv. Funct. Mater.* **2019**, *29*, No. 1901225.
(20) Yang, X.; Zhang, X.; Deng, J.; Chu, Z.; Jiang, Q.; Meng, J.; Wang, P.; Zhang, L.; Yin, Z.; You, J. Author Correction: Efficient Green Light-Emitting Diodes Based on Quasi-Two-Dimensional Composition and Phase Engineered Perovskite with Surface Passivation. *Nat. Commun.* **2018**, *9*, No. 1169.
(21) Vashishtha, P.; Ng, M.; Shivarudraiah, S. B.; Halpert, J. E. High Efficiency Blue and Green Light-Emitting Diodes Using Ruddlesden−Popper Inorganic Mixed Halide Perovskites with Butylammonium Interlayers. *Chem. Mater.* **2019**, *31*, 83−89.
(22) La-Placa, M.-G.; Longo, G.; Babaei, A.; Martínez-Sarti, L.; Sessolo, M.; Bolink, H. J. Photoluminescence Quantum Yield Exceeding 80% in Low Dimensional Perovskite Thin-Films Via Passivation Control. *Chem. Commun.* **2017**, *53*, 8707−8710.
(23) Chen, Z.; Zhang, C.; Jiang, X. F.; Liu, M.; Xiao, R.; Shi, T.; Chen, D.; Xue, Q.; Zhao, Y. J.; Su, S.; et al. High-Performance Color-Tunable Perovskite Light Emitting Devices through Structural Modulation from Bulk to Layered Film. *Adv. Mater.* **2017**, *29*, No. 1603157.
(24) Wang, N.; Chen, L.; Ge, R.; Zhang, S.; Miao, Y.; Zou, W.; Yi, C.; Sun, Y.; Cao, Y.; Yang, R.; et al. Perovskite Light-Emitting Diodes Based on Solution-Processed Self-Organized Multiple Quantum Wells. *Nat. Photonics* **2016**, *10*, 699−704.
(25) Huang, S.; Liu, N.; Liu, Z.; Zhan, Z.; Hu, Z.; Du, Z.; Zhang, Z.; Luo, J.; Du, J.; Tang, J.; Leng, Y. Enhanced Amplified Spontaneous Emission in Quasi-2d Perovskite by Facilitating Energy Transfer. *ACS Appl. Mater. Interfaces* **2022**, *14*, 33842−33849.
(26) Wang, Z.; Yang, J.; Li, M.; Zeng, X.; Pi, M.; Liu, Z.; Liu, J.; Zhang, D.; Hu, Z.; Du, J. Low Threshold and Ultrastability of One-Step Air-Processed All-Inorganic Cspbx(3) Thin Films toward Full-Color Visible Amplified Spontaneous Emission. *ACS Appl. Mater. Interfaces* **2022**, *14*, 26904−26912.
(27) Zhang, Y.; Dong, Z.; Ge, H.; Zhao, L. A.; Xu, H.; Wang, Y.; Song, L.; Xia, Y. Influence of the Surface Modification on Carrier Kinetics and Ase of Evaporated Perovskite Film. *IEEE Photonics Technol. Lett.* **2023**, *35*, 285−288.
(28) Ghaithan, H. M.; Qaid, S. M. H.; AlHarbi, K. K.; Bin Ajaj, A. F.; Al-Asbahi, B. A.; Aldwayyan, A. S. Amplified Spontaneous Emission from Thermally Evaporated High-Quality Thin Films of Cspb(Br(1-X)Y(X))(3) (Y = I, Cl) Perovskites. *Langmuir* **2022**, *38*, 8607−8613.
(29) Vaynzof, Y. The Future of Perovskite Photovoltaics—Thermal Evaporation or Solution Processing? *Adv. Energy Mater.* **2020**, *10*, No. 2003073.
(30) Cho, C.; Palatnik, A.; Sudzius, M.; Grodofzig, R.; Nehm, F.; Leo, K. Controlling and Optimizing Amplified Spontaneous Emission in Perovskites. *ACS Appl. Mater. Interfaces* **2020**, *12*, 35242−35249.
(31) Liang, Y.; Shang, Q.; Li, M.; Zhang, S.; Liu, X.; Zhang, Q. Solvent Recrystallization-Enabled Green Amplified Spontaneous Emissions with an Ultra-Low Threshold from Pinhole-Free Perovskite Films. *Adv. Funct. Mater.* **2021**, *31*, No. 2106108.
(32) Li, Y.; Allegro, I.; Kaiser, M.; Malla, A. J.; Richards, B. S.; Lemmer, U.; Paetzold, U. W.; Howard, I. A. Exciton Versus Free Carrier Emission: Implications for Photoluminescence Efficiency and Amplified Spontaneous Emission Thresholds in Quasi-2d and 3d Perovskites. *Mater. Today* **2021**, *49*, 35−47.
(33) Saidaminov, M. I.; Williams, K.; Wei, M.; Johnston, A.; Quintero, B. R.; Vafaie, M.; Pina, J. M.; Proppe, A. H.; Hou, Y.; Walters, G.; et al. Multi-Cation Perovskites Prevent Carrier Reflection from Grain Surfaces. *Nat. Mater.* **2020**, *19*, 412−418.
(34) Zhang, H.; Liao, Q.; Wu, Y.; Zhang, Z.; Gao, Q.; Liu, P.; Li, M.; Yao, J.; Fu, H. 2d Ruddlesden-Popper Perovskites Microring Laser Array. *Adv. Mater.* **2018**, *30*, No. 1703487.
(35) Li, M.; Zhou, J.; Tan, L.; Liu, Y.; Wang, S.; Jiang, C.; Li, H.; Zhao, X.; Gao, X.; Tress, W.; et al. Brominated Peai as Multi-Functional Passivator for High-Efficiency Perovskite Solar Cell. *Energy Environ. Mater.* **2022**, *0*, No. e12360.
(36) Peng, X.; Yang, X.; Liu, D.; Zhang, T.; Yang, Y.; Qin, C.; Wang, F.; Chen, L.; Li, S. Targeted Distribution of Passivator for Polycrystalline Perovskite Light-Emitting Diodes with High Efficiency. *ACS Energy Lett.* **2021**, *6*, 4187−4194.
(37) Guo, X.; Koh, T. M.; Febriansyah, B.; Han, G.; Bhaumik, S.; Li, J.; Jamaludin, N. F.; Ghosh, B.; Chen, X.; Mhaisalkar, S.; Mathews, N. Cesium Oleate Passivation for Stable Perovskite Photovoltaics. *ACS Appl. Mater. Interfaces* **2019**, *11*, 27882−27889.
(38) Shi, Y.; Li, R.; Yin, G.; Zhang, X.; Yu, X.; Meng, B.; Wei, Z.; Chen, R. Laser-Induced Secondary Crystallization of $Cspbbr_3$ Perovskite Film for Robust and Low Threshold Amplified Spontaneous Emission. *Adv. Funct. Mater.* **2022**, *32*, No. 2207206.
(39) Pourdavoud, N.; Haeger, T.; Mayer, A.; Cegielski, P. J.; Giesecke, A. L.; Heiderhoff, R.; Olthof, S.; Zaefferer, S.; Shutsko, I.; Hekei, A.; et al. Room-Temperature Stimulated Emission and Lasing in Recrystallized Cesium Lead Bromide Perovskite Thin Films. *Adv. Mater.* **2019**, *31*, No. 1903717.
(40) Li, J.; Si, J.; Gan, L.; Liu, Y.; Ye, Z.; He, H. Simple Approach to Improving the Amplified Spontaneous Emission Properties of Perovskite Films. *ACS Appl. Mater. Interfaces* **2016**, *8*, 32978−32983.
(41) Ou, J.; Guo, X.; Song, L.; Lin, J.; Lv, Y.; Fan, Y.; Li, Y.; Zou, D.; Bao, Z.; Liu, X. Ampholytic Interface Induced in Situ Growth of Cspbbr3 for Highly Efficient Perovskite Light-Emitting Diodes. *J. Mater. Chem. C* **2021**, *9*, 1025−1033.
(42) Peng, Q.; Guo, J.; Zhang, Q.; Xiang, J.; Liu, B.; Zhou, A.; Liu, R.; Tian, Y. Unique Lead Adsorption Behavior of Activated Hydroxyl Group in Two-Dimensional Titanium Carbide. *J. Am. Chem. Soc.* **2014**, *136*, 4113−4116.

https://doi.org/10.1021/acs.jpcc.3c05840
J. Phys. Chem. C 2023, 127, 21841−21848

(43) Liu, X.; Guo, X.; Lv, Y.; Hu, Y.; Fan, Y.; Lin, J.; Liu, X.; Liu, X. High Brightness and Enhanced Stability of $Cspbbr_3$-Based Perovskite Light-Emitting Diodes by Morphology and Interface Engineering. *Adv. Opt. Mater.* **2018**, *6*, No. 1801245.
(44) Yang, X.; Zhang, X.; Deng, J.; Chu, Z.; Jiang, Q.; Meng, J.; Wang, P.; Zhang, L.; Yin, Z.; You, J. Efficient Green Light-Emitting Diodes Based on Quasi-Two-Dimensional Composition and Phase Engineered Perovskite with Surface Passivation. *Nat. Commun.* **2018**, *9*, No. 570.
(45) Saparov, B.; Mitzi, D. B. Organic−Inorganic Perovskites: Structural Versatility for Functional Materials Design. *Chem. Rev.* **2016**, *116*, 4558−4596.
(46) Meng, L.; Yao, E. P.; Hong, Z.; Chen, H.; Sun, P.; Yang, Z.; Li, G.; Yang, Y. Pure Formamidinium-Based Perovskite Light-Emitting Diodes with High Efficiency and Low Driving Voltage. *Adv. Mater.* **2016**, *29*, No. 1603826.
(47) Qin, C.; Sandanayaka, A. S. D.; Zhao, C.; Matsushima, T.; Zhang, D.; Fujihara, T.; Adachi, C. Stable Room-Temperature Continuous-Wave Lasing in Quasi-2d Perovskite Films. *Nature* **2020**, *585*, 53−57.
(48) Qin, C.; Matsushima, T.; Potscavage, W. J.; Sandanayaka, A. S. D.; Leyden, M. R.; Bencheikh, F.; Goushi, K.; Mathevet, F.; Heinrich, B.; Yumoto, G.; et al. Triplet Management for Efficient Perovskite Light-Emitting Diodes. *Nat. Photonics* **2020**, *14*, 70−75.
(49) Ai, B.; Liu, C.; Deng, Z.; Wang, J.; Han, J.; Zhao, X. Low Temperature Photoluminescence Properties of Cspbbr3 Quantum Dots Embedded in Glasses. *Phys. Chem. Chem. Phys.* **2017**, *19*, 17349−17355.
(50) Tang, Y.; Guo, J.; Liu, B.; Qin, L.; Deng, Z.; Hu, Y.; Teng, F.; Lou, Z.; Hou, Y. Amplified Spontaneous Emission from Waveguides Based on Hybrid Quasi-2d Perovskites of Dion−Jacobson and Ruddlesden−Popper Phases. *J. Mater. Chem. C* **2023**, *11*, 10043−10050.
(51) Li, M.; Shang, Q.; Li, C.; Li, S.; Liang, Y.; Yu, W.; Wu, C.; Zhao, L.; Zhong, Y.; Du, W.; et al. High Optical Gain of Solution-Processed Mixed-Cation $Cspbbr_3$ Thin Films Towards Enhanced Amplified Spontaneous Emission. *Adv. Funct. Mater.* **2021**, *31*, No. 2102210.
(52) Alvarado-Leaños, A. L.; Cortecchia, D.; Folpini, G.; Srimath Kandada, A. R.; Petrozza, A. Optical Gain of Lead Halide Perovskites Measured Via the Variable Stripe Length Method: What We Can Learn and How to Avoid Pitfalls. *Adv. Opt. Mater.* **2021**, *9*, No. 2001773.
(53) Yakunin, S.; Protesescu, L.; Krieg, F.; Bodnarchuk, M. I.; Nedelcu, G.; Humer, M.; De Luca, G.; Fiebig, M.; Heiss, W.; Kovalenko, M. V. Low-Threshold Amplified Spontaneous Emission and Lasing from Colloidal Nanocrystals of Caesium Lead Halide Perovskites. *Nat. Commun.* **2015**, *6*, No. 8056.
(54) Chan, Y.; Steckel, J. S.; Snee, P. T.; Caruge, J. M.; Hodgkiss, J. M.; Nocera, D. G.; Bawendi, M. G. Blue Semiconductor Nanocrystal Laser. *Appl. Phys. Lett.* **2005**, *86*, No. 073102.
(55) Xiong, Q.; Huang, S.; Du, J.; Tang, X.; Zeng, F.; Liu, Z.; Zhang, Z.; Shi, T.; Yang, J.; Wu, D.; et al. Surface Ligand Engineering for Cspbbr3 Quantum Dots Aiming at Aggregation Suppression and Amplified Spontaneous Emission Improvement. *Adv. Opt. Mater.* **2020**, *8*, No. 2000977.

https://doi.org/10.1021/acs.jpcc.3c05840
J. Phys. Chem. C 2023, 127, 21841−21848